Nanoscale

RSC Publishing

PAPER

View Article Online
View Journal | View Issue

Cite this: *Nanoscale*, 2013, **5**, 12388

Self-assembled growth of multi-layer graphene on planar and nano-structured substrates and its field emission properties†

Jian-Hua Deng,*[a] Bin Yu,[a] Guo-Zheng Li,[a] Xing-Gang Hou,[a] Meng-Li Zhao,[a] De-Jun Li,[a] Rui-Ting Zheng[b] and Guo-An Cheng*[b]

Received 7th August 2013
Accepted 9th October 2013

DOI: 10.1039/c3nr04145j

www.rsc.org/nanoscale

Vertical multi-layer graphenes (MLGs) have been synthesized without a catalyst on planar and nano-structured substrates by using microwave plasma enhanced chemical vapor deposition. The growth of MLGs on non-carbon substrates is quite different from that on carbon-based substrates. It starts with a pre-deposition of a carbon buffer layer to achieve a homo-epitaxial growth. The nucleation and growth of MLGs was found to be strongly influenced by the surface geometry and topography of substrates. Planar substrates suitable for atom diffusion are favorable for growing large-scale MLGs, and defect-rich substrates are beneficial for quick MLG nucleation and thus the growth of densely distributed MLGs. The field emission properties of MLGs grown on planar and nano-structured substrates were studied and are found to be strongly dependent on the nature of substrates. Substrates having good conductivity and large aspect ratios such as carbon nanotubes (CNTs) have good field emission properties. The best field emission properties of MLG/CNT composites with optimal shapes were observed with a low turn-on electric field of 0.93 V μm^{-1}, a threshold field of 1.56 V μm^{-1}, a maximum emission current density of 60.72 mA cm^{-2}, and excellent stability.

Introduction

Graphene-based materials have attracted intensive interest over the past few years due to their outstanding electrical and mechanical properties and promising prospects in many novel applications.[1–3] With the impressive progress in research on single- and bi-layer graphenes, recent efforts are being made on graphene's multi-layer counterparts. Multi-layer graphene (MLG), having several to dozens of layers, is currently of great interest to scientists in various applications such as flexible organic memory devices,[4] n-type organic semiconducting devices,[5] field-effect transistors,[6] and photo-detectors.[7] Graphene is also considered as a promising field emission (FE) material due to its atomic sharp edges, incomparable conductivity, and excellent FE stability.[8–10] However, most graphenes, fabricated using traditional methods such as mechanical or chemical exfoliation of graphite,[1] epitaxial growth on SiC,[11] and chemical vapor deposition (CVD) on metal catalysts,[12–15] are lying down on the substrates. This morphology is believed to have little FE.[16] Thus the fabrication of vertical graphene is important to achieve a high-performance FE. Previous studies have proven that plasma enhanced chemical vapor deposition (PECVD) is the only way to synthesize vertical graphenes.[17–19] However, there are few attempts of fabricating graphene/one-dimensional-material composites such as graphene/nanowire and graphene/nanotube hybrids, and the nucleation and growth mechanism of vertical graphenes also needs to be further understood.

In the present paper, we adopted microwave PECVD to fabricate vertical MLGs both on planar and nano-structured substrates, studied the influences of surface geometry and topography of substrates on the growth of MLGs, and proposed MLG nucleation and growth mechanisms. FE properties of MLGs grown on different substrates were tested and are found to be strongly influenced by the nature of substrates.

Experimental details

Four types of substrates were adopted to grow MLGs. They are substrates with planar (Si wafers and 85 nm thick diamond-like carbon (DLC) film terminated Si wafers) and nano-structured surfaces (carbon nanotube (CNT) arrays and Si nanowire (SiNW) arrays). The Si wafers were treated with 4% dilute HF acid for 5 min to remove the SiO_2 termination. The DLC films were

[a]*College of Physics and Materials Science, Tianjin Normal University, Tianjin 300387, P. R. China. E-mail: jhdeng1983@163.com; Fax: +86-22-23766503; Tel: +86-22-23766503*

[b]*Key Laboratory of Beam Technology and Material Modification of Ministry of Education, Beijing Normal University, Beijing 100875, P. R. China. E-mail: gacheng@bnu.edu.cn; Fax: +86-10-62205403; Tel: +86-10-62205403*

† Electronic supplementary information (ESI) available: Experimental section, SEM images of MLGs grown on Si wafers and DLC films within 1 hour, and SEM and TEM images of MLG/CNT composites grown at 100 W. See DOI: 10.1039/c3nr04145j

deposited on the thus prepared Si wafers by using a metal vapor vacuum arc (MEVVA) ion source system.[20] The CNT arrays were grown by using a traditional thermal CVD method.[21] The SiNW arrays were prepared on the thus prepared Si wafers in a HF–$AgNO_3$ solution and a HF–H_2O_2 solution with Ag as the etching catalyst.[22] The microwave PECVD growth of MLGs was performed in a vacuum chamber at 800 °C, 1 kPa, and without a catalyst. C_2H_2 and H_2 were used as the carbon feedback and the carrying gas, respectively. The experimental details for sample preparation are given in ESI, S2–S4† and the corresponding images are shown in Fig. S1–S4.†

The prepared samples were characterized by scanning electron microscopy (SEM, S-4800, Hitachi, Japan, 10 keV), transmission electron microscopy (TEM, JEM-2010, JEOL, Japan, 200 kV), and Raman spectroscopy (LabRAM Aramis, Horiba Jobin Yivon, France, 633 nm) for structural information. Their work function was determined by using a photoelectron spectrometer (AC-2, Riken Keiki, Japan, spot area: 4×4 mm^2). The FE tests were carried out in an ultrahigh vacuum chamber by using a diode setup.[21] The experimental details for sample characterizations are given in ESI, S4 and S5† and the corresponding images are shown in Fig. S5 and S6.†

Results and discussion

Fig. 1 shows side-view SEM images of MLGs synthesized under the same growth conditions on the four types of substrates above mentioned. We chose a relatively large microwave power, 400 W, to promote the hydrogen etching and thus to reduce the amount of amorphous carbon on our products. MLGs grown on planar substrates, as shown in Fig. 1a and b and the corresponding insets, are found to be quite differently shaped. First, the height of MLGs on the Si wafers is nearly half of that on the DLC films. Second, the density of MLGs on the Si wafers is lower than that on the DLC films. These results indicate that the nucleation and growth of MLGs is substrate dependent. Furthermore, this difference in MLG density directly gives rise to the difference in MLG shapes. It can be seen that the MLGs grown on the Si wafers are semicircular having uniform height and width, both of which are about 250 nm, while for MLGs grown on the DLC films, the high density impedes their horizontal growth, resulting in the formation of a rectangular appearance (Fig. 1b). Considering the very difference in these two types of substrates is their surface topography, concretely, the distribution of intrinsic defects on the surfaces, we conjecture that the MLG growth is defect guided. Defect-rich substrates such as DLC films that facilitate MLG nucleation can accelerate the growth of MLGs. MLGs grown on nano-structured substrates have similar morphological characteristics to those in the planar substrates, as shown in Fig. 1c and d. Both the size and the density of MLGs grown on the CNT arrays are smaller than those on the SiNW arrays. This is attributed to the fact that the amount of intrinsic defects on the chemically etched SiNWs is larger than that on the CVD prepared CNTs. In addition, the surface geometry of substrates, which is characterized here in terms of planar and nano-structured, also influences the MLG shapes greatly. For example, comparing MLGs grown on the Si wafers (Fig. 1a) and CNT arrays (Fig. 1c), it can be found that the MLGs on the CNTs are much smaller than those on the Si wafers. We consider that the nano-structured nature of CNTs, which is detrimental to atom diffusion, impedes the formation of large-scale defects and thus limits the nucleation of large-scale MLGs.

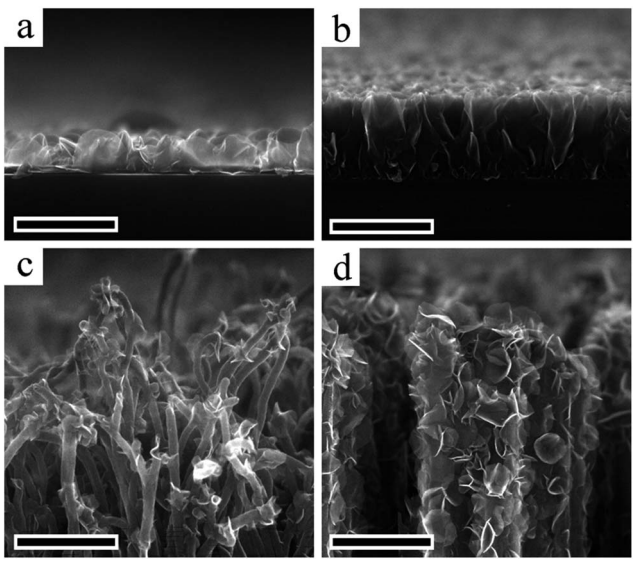

Fig. 1 Typical side-view SEM images of MLGs grown on substrates of (a) Si wafers, (b) DLC films, (c) CNT arrays, and (d) SiNW arrays, the insets are the corresponding top-view SEM images. Growth conditions: 400 W, 1 kPa, 800 °C, 5 sccm C_2H_2, 10 sccm H_2, and 5 hours. All the scale bars are 500 nm.

Observing the connection between MLGs and substrates can help us understand the growth of MLGs. In this regard, the fine structure of MLGs grown on CNT and SiNW arrays was observed by using a TEM. Fig. 2a shows dispersed MLG/CNT composites. The CNTs reserve their tubular structure and the small-scale MLGs are sparsely distributed, forming a rose-like appearance. Fig. 2b shows a TEM image of MLG/SiNW composites. It can be seen that the MLGs have a dense distribution on the SiNWs and they are almost transparent at the unfolded parts, indicating that our MLGs are ultrathin graphenes. The fine structure of a connection between a CNT and a MLG is shown in Fig. 2c. The clear atom arrangement in the connection demonstrates that the CNT and the MLG are chemically rather than physically bonded, thus the growth of MLG is self-assembled. Fig. 2d shows a high-resolution TEM image of MLGs grown on SiNWs. It can be seen that a carbon buffer layer is deposited on the rough surface of SiNWs before the growth of MLGs. We attribute this to the different compatibility in lattice between carbon and silicon. Since an MLG is composed of carbon, it needs a carbon bed to achieve a homo-epitaxial growth, the pre-deposition of a carbon buffer layer is thus essential before the growth of MLGs on SiNWs. The following MLG growth on this carbon layer is similar to that on the CNTs. The interlayer spacing of MLGs, in most cases, is similar to that of the bulk graphite gap (0.34 nm), as shown in Fig. 2e, but increases dramatically at the MLG tips (from 0.344 to 0.352 nm), mainly due to the decrease of the van der Waals

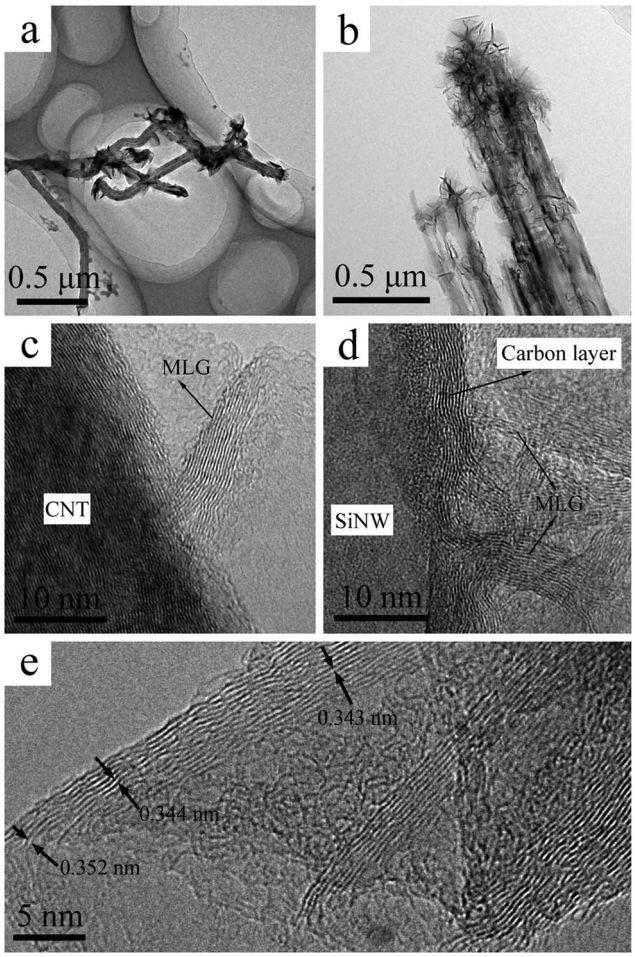

Fig. 2 (a and b) Low- and (c and d) high-resolution TEM images of MLGs grown on (a and c) CNTs and (b and d) SiNWs. (e) Typical high-resolution TEM image showing sharp MLG fringes.

interaction. It is interesting that the MLG, no matter the substrate is CNT or SiNW, has more than 10 layers at the bottom and 3–5 layers at the tips, which can be clearly seen in Fig. 2e. The reason for this is attributed to the inhomogeneous hydrogen plasma etching. The hydrogen plasma etching on the MLG tips is stronger than that on the bottom due to the shield from surrounding MLGs or CNTs or SiNWs. The outer layers at the MLG tips are thus peeled off by the hydrogen plasma, while the MLG bottom basically reserves its original shape that has been established during the nucleation stage.

Fig. 3 shows Raman spectra of MLGs grown on different substrates. All the MLG samples have three noticeable peeks. They are defect related D peak (~1335 cm^{-1}), graphitic carbon related G peak (~1580 cm^{-1}), and graphene related 2D peak (~2666 cm^{-1}).[23] The intensity ratio between the 2D peak and the G peak, *i.e.*, the I_{2D}/I_G ratio, is usually used to roughly estimate the thickness of graphenes. For example, the 2D peak of a single-layer graphene is roughly 4 times more intense than the G peak.[23] However, this evaluation only takes Raman signals from graphenes into consideration, which is inappropriate to the MLG/CNT system since the CNT also contributes to the Raman G peak. For the other three types of MLGs, the I_{2D}/I_G

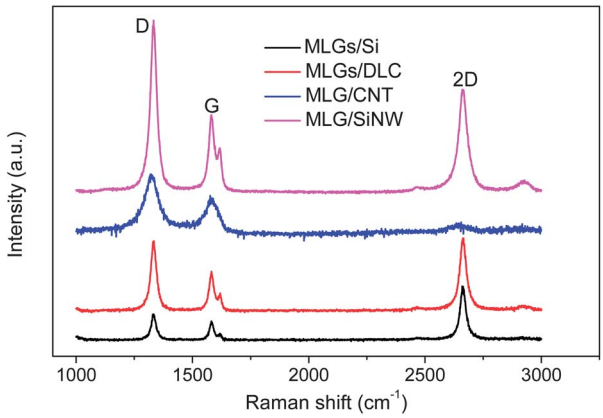

Fig. 3 Raman spectra of MLGs grown on Si wafers, DLC films, CNT arrays, and SiNW arrays. Laser wavelength: 633 nm.

ratios are larger than 1, indicating that our MLGs are ultrathin graphenes,[23] in good agreement with the TEM observations (Fig. 2c–e).

The nucleation and growth mechanism of MLGs on different substrates can be inferred on the basis of the above structural analyses. For carbon-based substrates such as CNTs and DLC films, as schematically shown in Fig. 4a, MLG nucleation starts at defects that are either intrinsic of substrates or generated due to hydrogen plasma etching, and then those defects grow by absorbing decomposited carbon atoms. The defect distribution on the surface of substrates directly influences the nucleation of MLGs. MLGs grown on defect-rich substrates, such as DLC films, nucleate more quickly than on defect-poor substrates, such as Si wafers, which can be evidenced by the SEM images of 1 hour MLG growth on these two substrates, as shown in Fig. S7.† Furthermore, the quick and dense nucleation of MLGs on defect-rich substrates greatly shields the hydrogen plasma etching on the graphenes and thus makes the MLGs grow higher. The MLG sizes are mainly determined by the scale of substrates. For example, CNTs, of 40–60 nm in diameter, greatly impede the diffusion of carbon atoms and thus impede the formation of large scale defects, resulting in the growth of MLGs with small sizes. The MLG size is also influenced by its density in the case of high-density nucleation such as the growth of

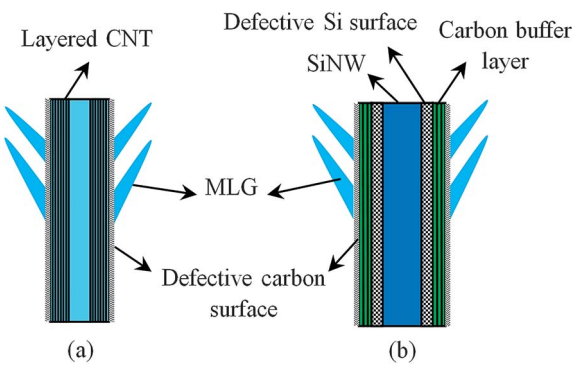

Fig. 4 Schematics of the growth of MLGs on (a) a CNT and (b) a SiNW.

MLGs on DLC films, as shown in Fig. 1b, resulting in limited MLG growth in the horizontal direction. For non-carbon substrates such as Si wafers and SiNWs, as schematically shown in Fig. 4b, the pre-deposition of a defective carbon buffer layer on the surface of substrates to achieve a homo-epitaxial growth is essential. The following MLG nucleation is similar to that on the carbon-based substrates. To summarize, the density and the size of MLGs are mainly determined by the surface topography (defect-rich or defect-poor) and the surface geometry (planar and nano-structured) of substrates.

The 2D growth of MLGs has been reported previously.[18,24–26] Based on their discussions, the surface diffusion length of a carbon atom on a flawless graphene before re-evaporation is:

$$\lambda_d = 2a_0 \exp\left(\frac{E_a - E_d}{2\kappa T}\right) = 2.33\ \mu m \quad (1)$$

where $a_0 = 0.14$ nm is the interatomic distance, $E_a = 1.8$ eV is the surface absorbing energy, and $E_d = 0.13$ eV is the surface diffusion energy, $T = 1073$ K the growth temperature and $k = 8.62 \times 10^{-5}$ eV K^{-1} the Boltzmann constant, for our MLG growth conditions. The λ_d here is far larger than the actual sizes of our MLGs, which are less than 500 nm in most cases. This is mainly due to the fact that the actual MLG growth conditions are quite different. Blocking from the existing defects on the surface of MLGs, prolonged diffusion length due to atom–atom collisions which are absent in the above assumption, together with the etching of hydrogen plasma, all of them impede the growth of MLGs.

The FE properties of the as-grown CNT and SiNW arrays, and MLGs grown on different substrates were measured for comparison (sample area ~0.04 cm^2, anode–cathode gap 1 mm). Fig. 5 plots the emission current density (J) of our samples as a function of the applied field (E), *i.e.*, the J–E curves. Samples shown in Fig. 5a have little FE. The turn-on electric fields at 10 μA cm^{-2} (E_{on}) and threshold fields at 1 mA cm^{-2} (E_{th-1}) are both large, and the maximum emission current density (J_{max}) are relatively small for these samples, as shown in Table 1. In comparison with the large E_{on} (6.50 V μm^{-1}) and E_{th-1} (7.51 V μm^{-1}) of the as-grown SiNW arrays, those of the MLG/SiNW composites are far smaller, indicating that the growth of MLGs on SiNWs can greatly improve their FE behavior. This is attributed, first, to the ultrathin MLGs that provide a great many effective emission sites and second, to a synergetic enhancement from the SiNWs and the MLGs that promotes the local electric fields at the emission sites. This promotion can be evidenced by comparing the FE properties of the MLG/SiNW composites with those of the MLGs grown on planar substrates: MLGs grown on the large-aspect-ratio SiNWs have superior FE to those on the planar Si wafers and DLC films with small aspect ratios. The work function of the MLG samples is smaller than that of the as-grown SiNWs, as shown in Table 1. The field enhancement factor (β), a geometric parameter of emitters, can thus be determined by the work function and the constant F–N slope in the low-current region,[27] as shown in the inset of Fig. 5a. The β of the MLG/SiNW composites is 1556, far larger than that of the other three samples, indicating that the superior FE of the MLG/SiNW composites is mainly attributed to their unique structure: thin MLGs and large-aspect-ratio SiNWs. It is interesting that the 500 nm high MLGs grown on DLC films (MLGs/DLC) have poorer FE than the 250 nm high MLGs grown on Si wafers (MLGs/Si). We attribute this to the influence of the field screening effect that decreases the actual local electric fields at the emission sites when the emitters are densely

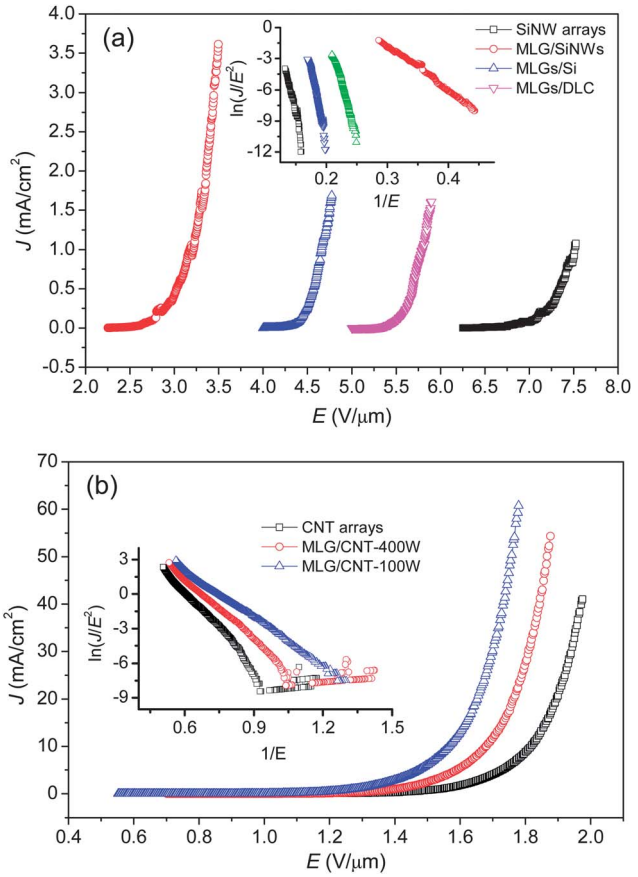

Fig. 5 (a) FE J–E (emission current density *versus* applied field) curves of SiNW arrays, MLG/SiNW composites, MLGs grown on Si wafers (MLGs/Si) and DLC films (MLGs/DLC). (b) FE J–E curves of CNT arrays and MLG/CNT composites synthesized at 400 and 100 W. The insets are the corresponding F–N plots, given in terms of $\ln(J/E^2)$ *versus* $1/E$.

Table 1 Turn-on (E_{on}, E at 10 μA cm^{-2}), threshold field (E_{th-1}, E at 1 mA cm^{-2}; E_{th-10}, E at 10 mA cm^{-2}), the maximum emission current density (J_{max}), work function (Φ) and field enhancement factor (β) of the SiNW and CNT arrays, and MLGs grown on different substrates

Samples	E_{on} (V μm^{-1})	E_{th-1} (V μm^{-1})	E_{th-10} (V μm^{-1})	J_{max} (mA cm^{-2})	Φ (eV)	β
SiNW arrays	6.50	7.51		1.08	5.07	212
MLG/SiNWs	2.45	3.17		3.61	4.72	1556
MLGs/Si	4.23	4.66		1.69	4.67	305
MLGs/DLC	5.29	5.80		1.61	4.70	232
CNT arrays	1.19		1.82	41.04	4.89	2954
MLG/CNT-400W	1.06		1.68	54.36	4.75	3721
MLG/CNT-100W	0.93		1.56	60.72	4.69	4625

packed,[28] which can be evidenced by the small β, 232, for the MLGs/DLC while 305 for the MLGs/Si.

The FE properties of the CNT samples are shown in Fig. 5b and Table 1. We presented here the FE of another CNT sample with relatively large-scale MLGs for comparison, which is named as MLG/CNT-100W composites. The SEM and TEM images of this sample are shown in Fig. S8.† It can be found that the FE behavior of the CNT samples is far better than that of the SiNW samples, the MLGs grown on planar substrates, and a great many well-verified good emitters such as single-layer graphene films,[29] single-crystalline boron nanowire arrays,[30] and single-crystalline Sb_2Se_3 nanowires,[31] which can be evidenced by their low E_{on} and E_{th-10} (E at 10 mA cm^{-2}) and large J_{max}, indicating that the FE characteristics of our emitters are mainly determined by the geometry of substrates. The CNTs that have large aspect ratios and excellent conductivity are beneficial for high-performance FE. The MLG/CNT composites have smaller work function than that of the as-grown CNT arrays, which is attributed to the ascended Fermi level induced by the increased state density of defects after the longtime plasma processing.[32] Similar to the MLG/SiNW composites, the growth of MLGs on CNTs greatly improves their FE, evidenced by the decreased E_{on} and E_{th-10} and the increased J_{max}. Compared to the small change of work function from 4.89 to 4.69 eV, the great change of the field enhancement factor from 2954 to 4625 after the growth of large-scale MLGs indicates that the FE of our emitters is mainly controlled by their geometric shapes. The MLG/CNT-100W sample presents excellent FE properties. It has a low E_{on} of 0.93 V μm^{-1} and E_{th-10} of 1.56 V μm^{-1}, and a large field enhancement factor of 4625. This excellent FE behavior is ascribed to the following aspects. Intrinsically, the MLGs have excellent conductivity, good mechanical properties, and atomic thin edges that yield large aspect ratios when the MLGs are not densely distributed, which satisfy all the requirements for a good field emitter. Furthermore, the carbon atoms at the MLG edges form distorted sp^3- rather than planar sp^2-hybridized geometry, which can decrease the barriers at the emission sites and thus facilitate the electron tunneling. These results are similar to those studies reported previously, where CNTs with open ends present better FE than closed ones.[33] Third, the CNT, composed of honeycomb carbon, also has excellent conductivity and mechanical properties and large aspect ratio due to its one dimensional nature. The self-assembled composition between these two materials will, basically, facilitate the electron transport, and consequently improve the FE performance. Fourth, in the case of composites with sparsely distributed MLGs, such as the MLG/CNT composites shown in our study, the field enhancement from the large-aspect-ratio CNT will not be shielded by the MLGs, which is helpful for promoting the local applied fields at the emission sites.

An aging process was taken before the FE stability tests. All the tested CNT samples have been aged at ~10 mA cm^{-2} for 5 hours to weaken influences such as absorbate induced promotion and Joule heating induced degradation on FE properties.[34,35] Generally, longtime stable FE at 10 mA cm^{-2} is believed to be a basic requirement for practical applications

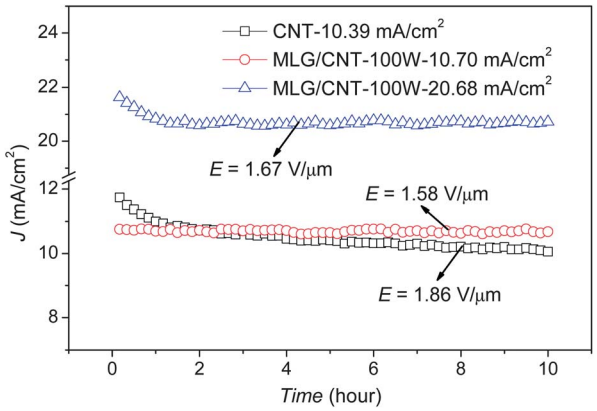

Fig. 6 FE stability of the as-grown CNT arrays and the MLG/CNT-100W composites at different constant electric fields within 10 hours.

such as fabricating flat panel displays. Fig. 6 shows the 10 hour FE stability of the as-grown CNT arrays and the MLG/CNT-100W composites at different constant applied fields, at which the emission current densities are larger than 10 mA cm^{-2}. We employ here a parameter J_{drop} to evaluate the stability. It is calculated by $(J_{first} - J_{last})/J_m$, where the J_{first}, J_{last}, and J_m are the first, the last, and the mean emission current density during the stability tests, respectively. The J_{drop} of the as-grown CNT arrays at ~10 mA cm^{-2} is 16.17% while it is only 0.69% for the MLG/CNT-100W composites. This is because for the one-dimensional CNTs, some protruded CNTs suffer from an excessive FE due to less field-screening and thus they are more likely to be burned off by Joule heat.[28,35] While for the MLGs, the unique two dimensional structure of which is advantageous for large current and faster heat dispersion, the Joule heating induced decrease of emission sites can thus be greatly weakened. Furthermore, the applied field of the MLG/CNT-100W composites at ~10 mA cm^{-2} is only 1.58 V μm^{-1}, far smaller than 1.86 V μm^{-1} of the as-grown CNT arrays, which is essential for practical applications. We further tested the FE stability of the MLG/CNT-100W composites at 20.68 mA cm^{-2} for 10 hours, as shown in Fig. 6. The J_{drop} is only 4.39%. It should be mentioned that this current degradation mainly occurs at the first hour, the J_{drop} in the last 9 hours is only 0.18%. Together with the relatively low applied field 1.67 V μm^{-1}, our MLG/CNT samples are expected to be applied in fields requiring longtime stable large-current FE.

Conclusions

We have demonstrated a catalyst-free growth of vertical MLGs both on planar and nanostructured substrates by using microwave PECVD. The growth of MLGs is greatly influenced by the surface topography and geometry of substrates. Defect-rich substrates such as SiNWs and DLC films facilitate the nucleation of MLGs, leading to the growth of MLGs with high density. Planar substrates suitable for atom diffusion are favorable for growing large-scale MLGs. The FE properties of MLGs are dependent on the nature of substrates. The large aspect ratio of

one-dimensional substrates such as CNT and SiNW is helpful for promoting the local applied fields at the emission sites of MLGs. MLG/CNT composites possessing the large aspect ratio of CNTs and the atomic thin edges of MLGs have excellent FE properties. The best FE properties of MLGs with optimal shapes were observed at the MLG/CNT-100W composites. They have a low E_{on} of 0.93 V μm^{-1} and E_{th-10} of 1.56 V μm^{-1}, a J_{max} of 60.72 mA cm^{-2}, and excellent FE stability (J decreases by 0.69% at 10.70 mA cm^{-2} and 4.39% at 20.68 mA cm^{-2} within 10 hours). Our results show that the MLG/CNT composites with sparsely distributed MLGs are promising for applications requiring longtime, stable, and large-current field electron emission.

Acknowledgements

This work was supported by the National Natural Science Foundation of China for Youth Science Funds (nos 51302187, 51302188, and 11204215), the National Basic Research Program of China (2010CB832905), the National Natural Science Foundation of China (51272176), the Tianjin High School Science & Technology Foundation (20120312), the Tianjin Natural Science Foundation (nos 13JCZDJC33900 and 12JCYBJC32500), and the Natural Science Foundation (5RL119), the Application Development Foundation (52XK1207), and the Youth Foundation (52XQ1204) of Tianjin Normal University.

Notes and references

1 K. S. Novoselov, A. K. Geim, S. V. Morozov, D. Jiang, Y. Zhang, S. V. Dubonos, I. V. Grigorieva and A. A. Firsov, *Science*, 2004, **306**, 666–669.
2 Y. M. Lin, C. Dimitrakopoulos, K. A. Jenkins, D. B. Farmer, H. Y. Chiu, A. Grill and P. Avouris, *Science*, 2010, **327**, 662.
3 J. S. Bunch, A. M. van der Zande, S. S. Verbridge, I. W. Frank, D. M. Tanenbaum, J. M. Parpia, H. G. Craighead and P. L. McEuen, *Science*, 2007, **315**, 490–493.
4 Y. Ji, S. Lee, B. Cho, S. Song and T. Lee, *ACS Nano*, 2011, **5**, 5995–6000.
5 Y. Yi, W. M. Choi, B. Son, J. W. Kim and S. J. Kang, *Carbon*, 2011, **49**, 4936–4939.
6 Y. Sui and J. Appenzeller, *Nano Lett.*, 2009, **9**, 2973–2977.
7 R. J. Sun, Y. Zhang, K. Li, C. Hui, K. He, X. C. Ma and F. Liu, *Appl. Phys. Lett.*, 2013, **103**, 013106.
8 M. Qian, T. Feng, H. Ding, L. F. Lin, H. B. Li, Y. W. Chen and Z. Sun, *Nanotechnology*, 2009, **20**, 425702.
9 I. Lahiri, V. P. Verma and W. Choi, *Carbon*, 2011, **49**, 1614–1619.
10 C. K. Huang, Y. X. Ou, Y. Q. Bie, Q. Zhao and D. P. Yu, *Appl. Phys. Lett.*, 2011, **98**, 263104.
11 C. Berger, Z. M. Song, X. B. Li, X. S. Wu, N. Brown, C. Naud, D. Mayou, T. B. Li, J. Hass, A. N. Marchenkov, E. H. Conrad, P. N. First and W. A. de Heer, *Science*, 2006, **312**, 1191–1196.
12 W. Li, C. Tan, M. A. Lowe, H. D. Abruna and D. C. Ralph, *ACS Nano*, 2011, **5**, 2264–2270.
13 A. Avsar, T. Y. Yang, S. Bae, J. Balakrishnan, F. Volmer, M. Jaiswal, Z. Yi, S. R. Ali, G. Güntherodt, B. H. Hong, B. Beschoten and B. Özyilmaz, *Nano Lett.*, 2011, **11**, 2363–2368.
14 K. S. Kim, Y. Zhao, H. Jang, S. Y. Lee, J. M. Kim, K. S. Kim, J. H. Ahn, P. Kim, J. Y. Choi and B. H. Hong, *Nature*, 2009, **457**, 706–710.
15 U. J. Kim, I. H. Lee, J. J. Bae, S. Lee, G. H. Han, S. J. Chae, F. Günes, J. H. Choi, C. W. Baik, S. I. Kim, J. M. Kim and Y. H. Lee, *Adv. Mater.*, 2011, **23**, 3809–3814.
16 Z. M. Xiao, J. C. She, S. Z. Deng, Z. K. Tang, Z. B. Li, J. M. Lu and N. S. Xu, *ACS Nano*, 2010, **4**, 6332–6336.
17 Y. H. Wu and B. J. Yang, *Nano Lett.*, 2002, **2**, 355–359.
18 M. Y. Zhu, J. J. Wang, B. C. Holloway, R. A. Outlaw, X. Zhao, K. Hou, V. Shutthanandan and D. M. Manos, *Carbon*, 2007, **45**, 2229–2234.
19 Y. Zhang, J. L. Du, S. Tang, P. Liu, S. Z. Deng, J. Chen and N. S. Xu, *Nanotechnology*, 2012, **23**, 015202.
20 J. H. Deng, S. L. Wu, P. C. Sun, R. T. Zheng, Y. Zhao and G. A. Cheng, *Diamond Relat. Mater.*, 2012, **25**, 45–49.
21 J. H. Deng, R. T. Zheng, Y. Zhao and G. A. Cheng, *ACS Nano*, 2012, **6**, 3727–3733.
22 K. Q. Peng, X. Wang and S. T. Lee, *Appl. Phys. Lett.*, 2008, **92**, 163103.
23 A. C. Ferrari, J. C. Meyer, V. Scardaci, C. Casiraghi, M. Lazzeri, F. Mauri, S. Piscanec, D. Jiang, K. S. Novoselov, S. Roth and A. K. Geim, *Phys. Rev. Lett.*, 2006, **97**, 197401.
24 B. Lewis and J. C. Anderson, *Nucleation and growth of thin films*, Academic Press Inc., London, 1979, p. 51.
25 O. A. Louchev, Y. Sato and H. Kanda, *Appl. Phys. Lett.*, 2002, **80**, 2752–2754.
26 Y. H. Lee, S. G. Kim and D. Tománek, *Phys. Rev. Lett.*, 1997, **78**, 2393–2396.
27 R. H. Fowler and L. Nordheim, *Proc. R. Soc. London, Ser. A*, 1928, **119**, 173–181.
28 S. J. Kyung, J. B. Park, B. J. Park, J. H. Lee and G. Y. Yeom, *Carbon*, 2008, **46**, 1316–1321.
29 F. Liu, J. F. Tian, L. H. Bao, T. Z. Yang, C. M. Shen, X. Y. Lai, Z. M. Xiao, W. G. Xie, S. Z. Deng, J. Chen, J. C. She, N. S. Xu and H. J. Gao, *Adv. Mater.*, 2008, **20**, 2609–2615.
30 T. Y. Zhai, M. F. Ye, L. Li, X. S. Fang, M. Y. Liao, Y. F. Li, Y. Koide, Y. Bando and D. Golberg, *Adv. Mater.*, 2010, **22**, 4530–4533.
31 Z. S. Wu, S. F. Pei, W. C. Ren, D. M. Tang, L. B. Gao, B. L. Liu, F. Li, C. Liu and H. M. Cheng, *Adv. Mater.*, 2009, **21**, 1756–1760.
32 G. Kim, B. M. Jeong and J. Ihm, *Appl. Phys. Lett.*, 2006, **88**, 193107.
33 J. M. Bonard, H. Kind, T. Stockli and L. A. Nilsson, *Solid-State Electron.*, 2001, **45**, 893–898.
34 A. Maiti, J. Andzelm, N. Tanpipat and P. von Allmen, *Phys. Rev. Lett.*, 2001, **87**, 155502.
35 K. A. Dean, T. P. Burgin and B. R. Chalamala, *Appl. Phys. Lett.*, 2001, **79**, 1873–18l75.